Contrib Mineral Petrol (1999) 136: 273–284

D.A. Schneider · M.A. Edwards
P.K. Zeitler · C.D. Coath

Mazeno Pass Pluton and Jutial Pluton, Pakistan Himalaya: age and implications for entrapment mechanisms of two granites in the Himalaya

Received: 31 August 1998 / Accepted: 10 March 1999

Abstract Zircon and monazite U-(Th)-Pb ion microprobe analysis were performed on the Mazeno Pass pluton and the Jutial pluton, two leucogranite bodies within the Nanga Parbat-Haramosh massif (NPHM), Pakistan Himalaya. Zircon rim ages and monazite ages indicate the Mazeno Pass pluton in southwest NPHM intruded at 1.40 ± 0.05 Ma; the Jutial pluton, to the north, similarly yields concordant zircon and monazite ages suggesting crystallization at 9.45 ± 0.06 Ma. The Jutial pluton was subsequently intruded by leucogranite dikes at 5.3 Ma, as revealed by monazite ages. Concordancy of U-Pb and Th-Pb accessory mineral ages demonstrates the robustness of the technique on young rocks. Both plutons, some of the youngest in the Himalaya, have a general association with nearby shear zones that we interpret to have played an integral role in granite evolution and emplacement setting ('deformation enhanced ascent'). Together with new field observations, these results provide an insight on the spatial and temporal relationship between plutonism and deformation relating to the development of the massif.

D.A. Schneider (✉) · P.K. Zeitler
Department of Earth and Environmental Sciences,
Lehigh University, Bethlehem, Pennsylvania, 18105, USA
e-mail: dasd@lehigh.edu; pkz0@lehigh.edu

M.A. Edwards[1]
Department of Earth and Atmospheric Sciences,
State University of New York, Albany, New York, 12222, USA

C.D. Coath
Department of Earth and Space Sciences,
University of California, Los Angeles, California, 90095, USA
e-mail: coath@oro.ess.ucla.edu

Present address:
[1]Institut fuer Geologie, Universtaet Wuerzburg,
Wuerzburg, Germany
email: edwards@geologie.uni-wuerzburg.de

Editorial responsibility: T.L. Grove

Introduction

Along the >2500 km Himalaya orogen, field mapping and isotopic age data have revealed important space-time patterns of plutonism associated with thrusting, metamorphism and, indirectly, extension. The apparent coincidence of these inherently linked tectonic processes has lead many authors to invoke several tectonomagmatic models over the past score or so of years (e.g. decompression melting, shear heating, dehydration melting, etc.: Le Fort 1975, 1981; Debon et al. 1985; Le Fort et al. 1987; Zeitler and Chamberlain 1991; Harris and Massey 1994; Scaillet et al. 1995; Harrison et al. 1998). The High Himalayan granites are considered to be the result of anatexis of the Tibetan Slab rocks and imbricated portions of the North Indian margin (e.g. Le Fort et al. 1987), and granites of the central section of the orogen have received the majority of attention (e.g. Gangotri, Manaslu, Rongbuk-Makalu, Khula Kangri). Intrusion ages are typically Early Miocene (e.g. Le Fort et al. 1987; Harrison et al. 1995) or Middle Miocene (Edwards and Harrison 1997) for the eastern Himalaya. Recent debates involving the relationship between plutonism, high topography and the Himalayan detachment system suggest a coupling between plutonism and tectonic deformation that is associated with orogenic collapse (Molnar et al. 1993; Fielding 1996, Murphy and Harrison 1998).

Recently, in other orogenic belts (e.g. Seward Peninsula, Alaska; Coast Ranges, British Columbia; Papua New Guinea) several authors have emphasized the association of plutonic activity with the development of syn- to late-orogenic structures (e.g. Hollister and Crawford 1986; Hill et al. 1992; Baldwin et al. 1993; Amato et al. 1994). Such studies generally conclude that granitoids are emplaced and guided by shear zone geometry and that plutonism provides a rheological weakening mechanism that further enhances localized strain, accelerating deformation along principal shears. This typically creates a dynamic condition or 'positive

feedback' (Brown 1994). One result is a close temporal concordancy of pluton emplacement and of the cooling of the associated high-grade metamorphic terranes transported upward during uplift (e.g. Hollister and Crawford 1986).

The northwest Himalaya syntaxis, where the main Himalayan chain terminates, includes the Nanga Parbat-Haramosh massif. Previous Himalayan leucogranite crystallization ages from northwestern Pakistan, determined by U-(Th)-Pb ion microprobe dating of zircons and monazites, are younger then those reported elsewhere in the Himalaya; undeformed dikes within the massif give accessory mineral ages between <2 and 7 Ma (Zeitler and Chamberlain 1991; Schneider et al. 1997) and the Tato pluton yields zircon rim ages of $\sim$1 Ma (Zeitler et al. 1993). We present here the youngest monazite ages yet reported for a granite intrusive into the westernmost Himalayan crystallines: the Mazeno Pass Pluton. We analyzed the Mazeno Pass pluton to constrain further the young magmatism around the Nanga Parbat summit. Also dated was the Jutial pluton, located in the northwest corner of the massif. Both the Mazeno Pass pluton and the Jutial pluton are adjacent to the principal uplift-related (Edwards et al. 1996, 1997; Edwards 1998; Schneider et al. in press) structures; subsequent to reporting our geochronology and field relationships, we discuss the implications of our data with respect to granite intrusions into shear zones. It is through geochronologic and structural investigation of plutons situated near and within shear zones (e.g. Solar et al. 1998) that the association between deformation and magmatism can be understood.

Regional geology

The Nanga Parbat-Haramosh massif (NPHM) is central to the India-Asia collisional orogen in northern Pakistan (Fig. 1), the NW physiographic termination of the Himalayan chain marked by the peaks Nanga Parbat (8125 m) and Haramosh (7397 m). The NPHM consists of Indian rocks locally exhumed from beneath a fossil island arc terrane, the Kohistan-Ladakh arc (KLA), a series of late Cretaceous and Eocene amphibolites, volcanics and plutons (Tahirkheli et al. 1979; Coward et al.

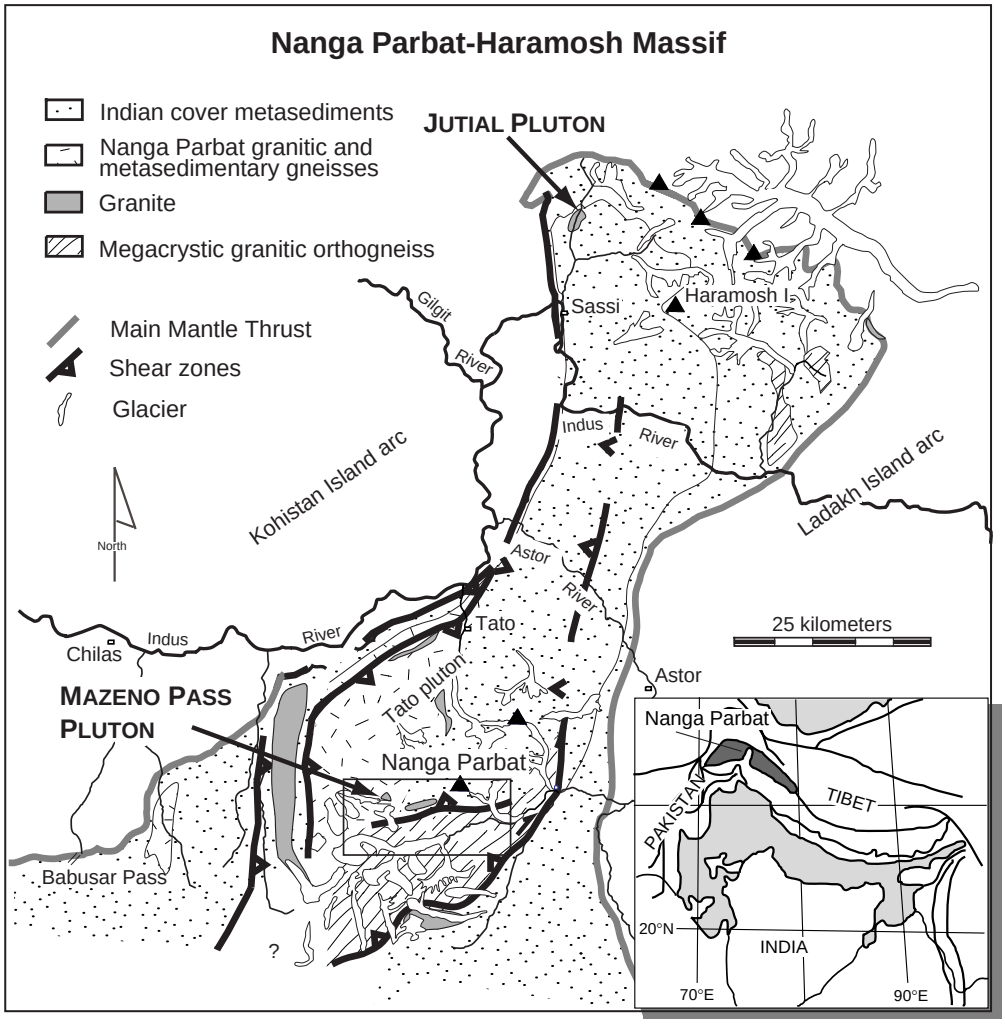

Fig. 1 Gerologic map of the Nanga Parbat-Haramosh massif (after Edwards, Kidd, Khan, and Schneider unpublished mapping). Boxed area in southern Nanga Parbat is location of Fig. 2. Inset: simplified regional tectonic schematic map of the Himalayan orogenic system showing the island arc terrane (*dark gray*) and the Nanga Parbat massif. *Light gray* regions are foreland basins

1982). The KLA is separated from the Himalayan rocks by the Main Mantle Thrust (MMT; Tahirkheli et al. 1979) whose surface trace forms a large bend around NPHM. The massif is a tectonic half window exposing Early Proterozoic gneisses of the Indian plate and Indian passive margin metasediments. The syntaxis area also marks the general region of orogenic kinking around which the Himalayan chain bends and is characterized by the presence of crustal-scale north-trending antiformal structures (Hazara, NPHM) which deform the main Himalayan thrusts (e.g. Wadia 1932; Misch 1949; Treloar et al. 1989; Butler et al. 1989). It is now recognized that a north-trending pop-up structure (Edwards et al. 1996, 1997; Edwards 1998) is associated with the relative uplift of NPHM and hence with the bend in the trace of the MMT, whereby late major Himalayan shear zones northwest (Madin 1986; Butler and Prior 1988; Madin et al. 1989) and southeast (Edwards et al. 1996, 1997; Schneider et al. 1997) of the main massif are responsible for exposure of the NPHM.

Nanga Parbat's metamorphic and magmatic history remains somewhat enigmatic because the massif is a largely reworked, high-grade terrane that, until recently, lacked direct evidence for Himalayan-aged metamorphism and plutonism [Schneider et al. 1999 present evidence for typical Himalayan (Early Miocene) anatexis in southern Nanga Parbat, obtaining monazite and zircon ages of ~19 Ma from the Southern Chichi pluton, indicating Nanga Parbat has a complex and protracted tectonic history]. The latest episode of high-grade amphibolite to granulite metamorphism of the Indian plate orthogneisses, paragneisses and metasediments is Late Miocene and younger (Smith et al. 1992). Rocks from within the core of the massif are frequently migmatized and yield an overall decompression path from 6.0 ± 1 kbar (600 ± 100 MPa) at 650 ± 50 °C to 4.1 ± 1 kbar (410 ± 100 MPa) at 600 ± 50 °C (Zeitler et al. 1993; Winslow et al. 1995). In Tato, the pressure estimates for the migmatization of the rocks at ~4.5 kbar (~450 MPa) have been combined with U-Pb monazite ages for these rocks of 3.3 Ma to obtain an exhumation rate of 4.5 ± 1.1 km per million year (Zeitler et al. 1993). Winslow et al. (1994) utilized $^{40}Ar/^{39}Ar$ ages on biotite and fluid inclusion data to obtain an exhumation rate of about 5 km per million years over the past 1 million years. Unlike the main Himalaya, no evidence for major regional extensional unroofing has been found within the NPHM, despite extensive field investigation at NPHM (Edwards 1998; Schneider et al. in press). Along strike of the orogen, the first known occurrence of a major extensional detachment is ~150 km to the southeast in Indian Himalaya (Zanskar Shear Zone; Herren 1987). Cooling and exhumation was nevertheless extremely rapid, with most thermochronometers yielding ages < 10 Ma (Winslow et al. 1996). The pattern of cooling ages must reflect erosional denudation of the north-plunging pop-up structure (Winslow et al. 1996; Edwards et al. 1996).

Scattered leucogranites (< 10% of exposed rock) intrude the massif, having most likely been generated by partial melting of pelitic rocks of the Indian continent crust (George et al. 1993; Harris and Massey 1994). Previously reported compositions (e.g. George et al. 1993) and our own data show that these igneous rocks (loosely termed leucogranites in the literature) range from granite to granodiorite to tonalite in composition. Additionally, crystallization ages are contemporaneous with metamorphism and deformation. One of the larger bodies, the Tato pluton, intruded local gneisses at ~1 Ma (Zeitler et al. 1993). Tourmaline-pegmatites are also present as < 2 meter-wide dikes throughout NPHM. Accessory mineral U-Th-Pb ages from dikes within the massif are 7–5 Ma in the northern and central portions (Zeitler and Chamberlain 1991) and 2.7–1.3 Ma closer to the summit (in Tato, Zeitler and Chamberlain 1991, and in Rupal, Schneider et al. 1997). Decompression melting of adjacent country rock due to rapid Tertiary denudation (Zeitler and Chamberlain 1991) under water-undersaturated conditions (Butler et al. 1997) has been suggested as the mechanism for the formation of the younger leucogranite sheets.

Local geology

Jutial Pluton

Located in the northwestern portion of the NPHM (Fig. 1), the Jutial granite is predominantly a two-mica ± tourmaline granite and is essentially undeformed. The granite locally has a weak preferred orientation of quartz grains, sutured grain boundaries and secondary muscovite growth (Butler et al. 1992). It intrudes the surrounding quartzofeldspathic Nanga Parbat gneisses, cross-cutting the generally north-south fabric. The trace element contents, Rb/Sr, and Sr and Nd isotope systematics suggest (1) that the source of the granite is similar to the gneisses currently exposed at Nanga Parbat (Inger and Harris 1993; George et al. 1993) and (2) the Jutial pluton has a similar petrogenesis to other High Himalayan leucogranites (Butler et al. 1992). The size of the body is difficult to determine, but our field observations suggest a diameter of at least 5 km. The main body of the Jutial pluton has been reported to be a minimum-melt granite (Butler et al. 1992) containing up to 10% each of biotite and muscovite. Observations by Butler and coworkers (Butler et al. 1992; George et al. 1993), suggest that at least two phases of intrusion within the main body can be distinguished: a main phase and a secondary cross-cutting phase, described as smaller (1–2 m) equigranular granitic sheets which cross-cut the margins of the pluton. The samples that we collected from the main body of the Jutial pluton and have used for analyses are: (J-1) a medium grained, tourmaline speckled granite, and (J-2) a pegmatitic version of what petrologically appears to be the same rock. A cross-cutting igneous phase of the Jutial granite (that we assume to be the secondary cross-cutting phase of Butler et al. 1992) was also examined and sampled for analyses (J-4) near the village of Jutial. This phase of the granite includes books of muscovite but overall has less muscovite than the main body. Additionally, in this phase gem quality tourmaline is euhedral and roughly equigranular (1–2 cm) and is distributed homogeneously throughout the rock. Tourmaline is observed in many Himalayan leucogranites and probably reflects varying water activity and boron concentrations during crystallization (Scaillet et al. 1991). The petrology of this second, pegmatitic rock is similar to the very young leucogranites of the southern portions of the massif in Rupal valley (Schneider et al. 1997).

Previous geochronologic studies report biotite and muscovite $^{40}Ar/^{39}Ar$ cooling ages from the Jutial granite are ~5–6 Ma (George et al. 1995) and George et al. (1993) reported a Rb/Sr muscovite age for the Jutial granite of 6.5 Ma.

Mazeno Pass Pluton

To the southwest of the summit region of Nanga Parbat, Mazeno Pass (5400 m) allows passage from Rupal valley, southern Nanga Parbat, to the north-south trending Bunar valley, west of Nanga Parbat (Fig. 2). Recent mapping in southern Nanga Parbat (Edwards et al. 1996; Edwards 1998; Schneider et al. in press) shows extensive, widely distributed granitic orthogneiss bodies, parts of which mark crustal-scale shear zones. On the northwest face of Mazeno Pass, the Mazeno Pass pluton is a notably undeformed, tourmaline-absent, fine-grained, muscovite ± biotite granite which cross-cuts the fabric of local biotite-rich, quartzofeldspathic gneiss whose layering trends ~north-northeast, dipping steeply west. The pluton was intruded into the northwest margin of a several km-wide belt of granitic S-C orthogneiss, interpreted to be a major shear zone, the Rupal shear (Edwards et al. 1996; Edwards 1998). The pluton is > 300 m thick and > 500 m wide and is exposed over much of the cirque wall. Leucogranite dike offshoots, of a few meters thickness, radiate away from the margins of the pluton trending northeast and dipping moderately to steeply to both the northwest and southeast. The offshoots are observed in some places to cross-cut tourmaline bearing pegmatite dikes/sheets dipping largely to the north, similar to those dikes seen in Upper Rupal valley. Locally, significant cordierite-bearing leucogranite float was seen at Mazeno Pass, probably carried by glaciers descending from the summit. Cordierite-bearing granitic veins and migmatites formed as partial melts during the recent high-grade metamorphism under water-saturated conditions (Whittington et al. 1999). We did not observe any pluton offshoots cross-cutting the cordierite-bearing bodies, nor cordierite-bearing bodies cross-cutting the main body or its offshoots. Sample E610-A (MAZ in Table 2) was taken from the main body for geochronologic analysis.

Analytical techniques

Single-grain, single-spot U-Pb and Th-Pb ages were measured using the CAMECA ims 1270 ion microprobe facility at University of California, Los Angeles following the analytical methods described by Harrison et al. (1995). The primary ion beam is O^- and was focused to a 15 × 20 μm ellipse. Accessory mineral ages and errors reported here are calculated as weighted averages; errors here are reported as $\pm 2\sigma$. The precision of the method is not limited by counting statistics but by the reproducibility of the standard calibration curve which is typically ±1% to 2% (Harrison et al. 1995). U-Pb zircon ages were determined relative to zircon standard AS3 (1099 ± 1 Ma) and Th-Pb monazite ages were determined relative to monazite standard 554 (45 ± 1 Ma). Uranium and thorium concentrations were estimated semiquantitatively by comparing peak heights in the unknowns to that in standards AS3 and 554, which have mean concentration of ~400 ppm and ~40000 ppm, respectively.

Chemical fractionation of radioactive daughter nuclides from their primary radioactive parents ^{238}U and ^{235}U is potentially an important cause for radioactive disequilibrium in young rocks such as in Nanga Parbat. Element partitioning between a magma and its source changes the proportion of intermediate radioactive daughters relative to their parent nuclides in both magma and crystallizing solids. Enrichment of intermediate isotopes relative to their equilibrium concentration leads to excess, and depletion leads to diminished production of stable end members ^{206}Pb and ^{207}Pb compared to production under equilibrium conditions (Barth et al. 1989). Subsequently, the U-Pb data for young systems have to be corrected for these initial deviations from secular equilibrium; this correction procedure is complex and requires assumptions about true inital abundances and mineral/melt fractionation.

This potential problem of disequilibrium, however, can be circumvented by dating minerals with elevated Th concentrations, like monazite, via the $^{208}Pb/^{232}Th$ method. Because secular equilibrium among the intermediate daughter isotopes of ^{232}Th is attained within ~30 years, it is unlikely that monazite will contain unsupported ^{208}Pb (Harrison et al. 1995). This gives an advantage to the $^{208}Pb/^{232}Th$ method over the traditional U-Pb method in young rocks. Harrison et al. (1995) have developed a methodology that permits precise (±2%) Th-Pb dating of young monazites using the ion microprobe. Moreover, prior studies of Nanga Parbat monazites (e.g. Smith et al. 1992), and backscattered electron/scanning electron microscope (BSE/SEM) images in this study indicate that the Nanga Parbat monazites in general are homogeneous and probably the result of primary formation and not the crystallization from a non-metamorphic, rare earth element (REE)-rich fluid.

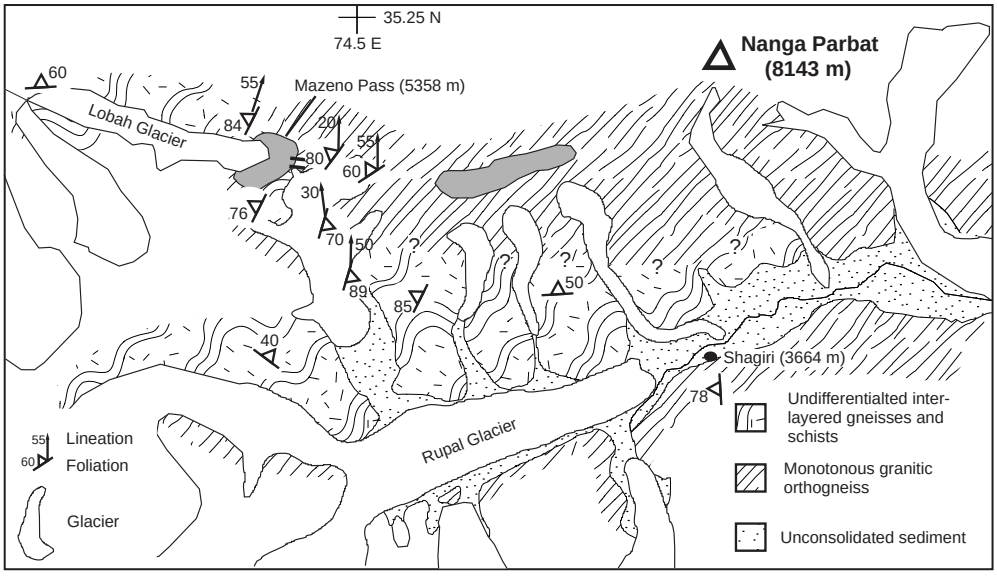

Fig. 2 Local map of Upper Rupal Valley and Mazeno Pass. Granite represented by *gray shaded* regions. The monotonous orthogneiss contains 0.25–2.0 cm felsic porphyroclasts frequently augen-shaped due to development of C/S fabric. The undifferentiated unit contains meter-scale compositionally layered gneiss with no obvious metasedimentary rocks present. Nature of the "contact" between two units is not clear. The oblate granitoid body east of Mazeno Pass is visible from the pass and not accessible

Results

Uranium-Pb zircon and $^{208}Pb/^{232}Th$ monazite analyses from the Mazeno Pass pluton and the Jutial pluton place significant constraints on the timing of pluton crystallization at NPHM. Results are plotted in Fig. 3 with Tables 1 and 2 listing isotopic data. From the Mazeno Pass pluton, sample E610-A, we measured 20 U-Pb ages on 6 zircon grains (200–500 μm) and 7 Th-Pb ages on 5 monazite grains (100–200 μm). The zircons are clear to white euhedral grains and the monazites are greenish yellow anhedral grains. For the Jutial pluton, three samples from the main body of the pluton were analyzed: 18 U-Pb ages on 10 zircons (< 100–300 μm) from two different samples (J-1, J-2) as well as 6 Th-Pb ages on 5 monazite grains (100–200 μm) from one of the two samples (J-2) and 11 Th-Pb ages on 7 monazite grains (100–200 μm) from a third sample (J-4). Both Jutial zircon separates are cloudy, bluish-green, generally euhedral grains and the monazites are transparent green.

Jutial Pluton results

All but four analyses (J-2_gr3sp1@2, J-2_gr3sp2, J-1_gr1sp2, and J-1_gr4sp1) of zircons from the Jutial pluton yield ~10 Ma ages (Fig. 3). Samples J-1 and J-2 together yield a weighted average zircon $^{206}Pb/^{238}U$ age of 9.54 ± 0.37 Ma (N = 14 spots); disregarding data outliers, which are the three youngest and three oldest ages, yields a weighted average zircon $^{206}Pb/^{238}U$ age of 9.39 ± 0.13 Ma (N = 8 spots). The $^{207}Pb/^{235}U$ uncertainties are large in all cases, sometimes as large as 50%, and within those uncertainties, the analyses are concordant.

Four of the spot analyses not used in the weighted average age plot well above the ~10 Ma cluster (at 15 Ma) and sometimes parallel concordia, leading to an apparent spread in the concordant ages. A number of explanations exist that can explain this behavior. To explore possible explanations, we conducted further investigation with the ion microprobe. These anomolously older ages are consistent with areas within the grains that contain high concentrations of P, Y, and Ca and lack Zr. Yttria can commonly be present in zircons and this can be related to the isostructural relationship of xenotime (YPO_4) and zircon (Deer et al. 1966). These elements indicate inclusions of xenotime or apatite (calcium phosphate) within the zircon so casting doubt on the reliability of the these particular ion microprobe U-Pb spot ages and giving rise to the apparent age spread.

Alternatively, each of our zircon ages might represent the crystallization age of the analyzed zircon and the spread therefore reflects extended zircon growth within the pluton. Previous workers (Jaupart and Provost 1985; Le Fort et al. 1987) have demonstrated dynamic conditions capable of generating melts from a source region for a protracted period of time (10–20 million years). Additionally, with such a scenario, an evolving melt that is crystallizing (and fractionating) would become saturated in Zr early in its genesis and reveal a range of zircon ages as a result (Harrison and Watson 1983; Watson and Harrison 1983). However, due to the rapid nature of denudation within the massif, especially along the western margin, it is difficult to see how the source region maintained a region of partial melting conditions for ~5 million years without invoking an external catalyst (deformation?). Thus we suggest that the spread in ages is due in part to microscopic inclusions and possibly xenocrystic contamination which can be seen with BSE/SEM; accordingly we infer that the crystallization age for the Jutial pluton is ~9.5 Ma.

Our inferred age is further supported by monazite $^{208}Pb/^{232}Th$ analyses from the latter sample, J-2 (Table 1). A weighted average monazite age of 5 of the 6 spots is 9.51 ± 0.12 Ma. It has been shown that even at the high melting temperatures required to produce granites, Pb diffusion in monazites is sufficiently sluggish to ensure recording crystallization ages (Smith and Giletti 1997; Edwards and Harrison 1997). Subsequently, with the concordant zircon and monazite ages, we confidently assign 9.45 ± 0.06 Ma as the emplacement age of the main body of the Jutial granite. It is interesting to note that even though zircon cores were analyzed, the ages reflect no Early Proterozoic (~1850 Ma) inheritance as present in other U-Pb zircon studies from Nanga Parbat (e.g. Mazeno Pass pluton this study; Zeitler et al. 1989; Zeitler et al. 1993; Schneider et al. 1999; Schneider unpublished data). This may indicate a northward decrease in the ancient crustal signature.

Sample J-4, the cross-cutting phase, yielded a monazite Th-Pb weighted average age of 5.27 ± 0.07 Ma (N = 9) (Table 1). We suggest that this leucogranite is similar to the dikes/sheets in the Indus and Astor River sections studied by Zeitler and Chamberlain (1991) yielding accessory mineral ages between 5 and 7 Ma.

Mazeno Pass Pluton results

Uranium-Pb zircon analyses of sample E610-A fall along a chord (Fig. 3) with an upper intercept and concordant core analysis of ~1860 Ma, representing the Precambrian protolith age, seen elsewhere within the re-worked NPHM gneisses (Zeitler et al. 1989) and Tato and Southern Chichi plutons (Zeitler et al. 1993; Schneider et al. 1999); this age is consistent with the protolith age of nearby gneisses and schists (Schneider et al. 1997). The lower intercept is defined by a cluster of concordant $^{206}Pb/^{238}U$ zircon rim ages at 1.35 ± 0.05 Ma.

Numerous investigations have shown that U-Pb systematics in zircons can survive metamorphism, partial melting, and even assimilation into magmas, and complete resetting of the ages of a zircon population seems to require dissolution and new growth of zircon (Sobolev and Shatsky 1990; Claoue-Long et al. 1991). Temperatures

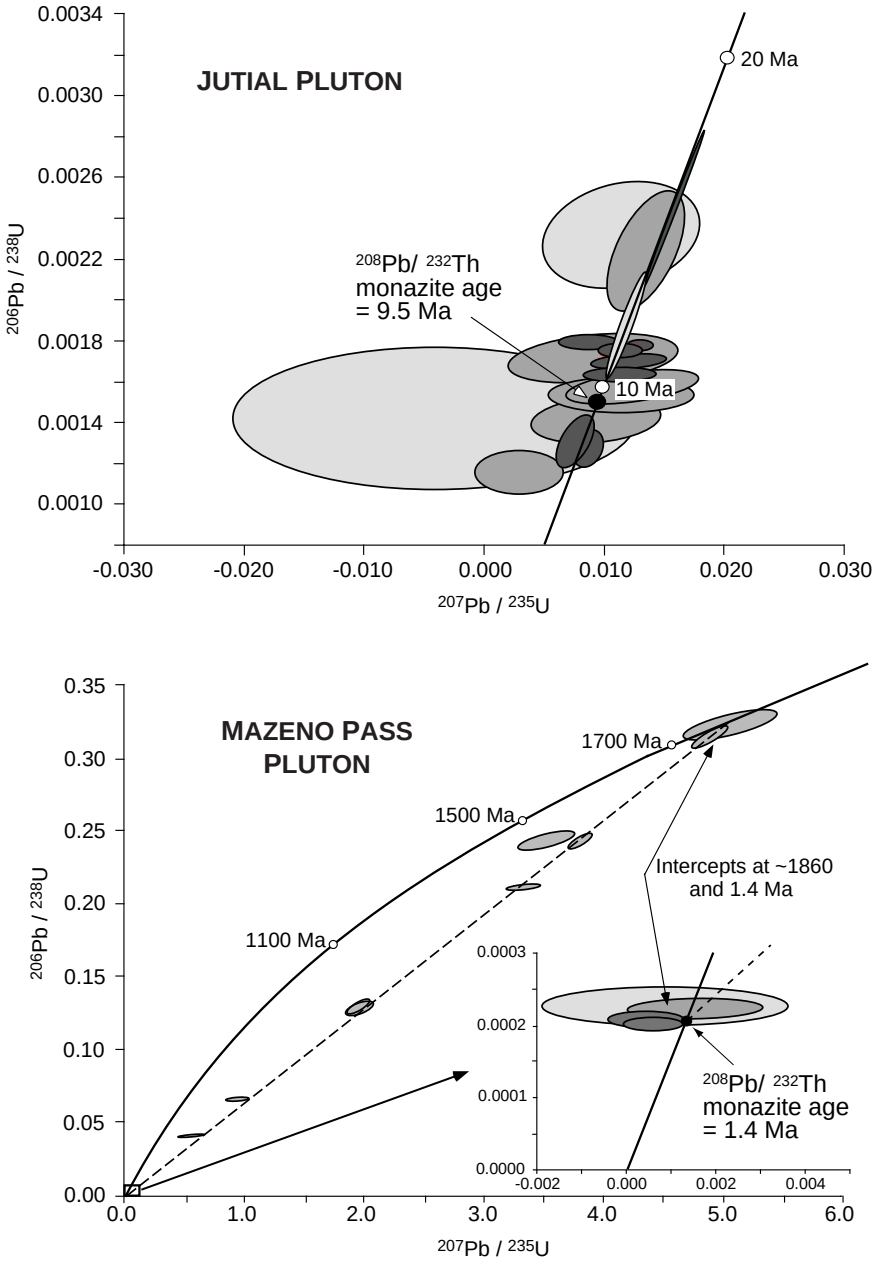

Fig. 3 U-Pb concordia plots showing zircon analyses of the Jutial and Mazeno Pass plutons. Error ellipses are shown at the 1σ level. Also plotted (as *black circles*) are the results of the Th-Pb monazite analyses. Inset of Mazeno Pass data shows enlarged concordia origin. Shading of ellipses is for viewing purposes

in excess of 1000 °C must be inferred for Pb-loss from pristine zircons (Williams 1992). Lead-diffusion experiments support this hypothesis, where it has been shown that pristine zircons with low U-content (< a few ppt) give off their radiogenic Pb slowly at ~1600 °C as a result of breakdown of zircon into baddeleyite and SiO_2, and not as a result of diffusion. Chapman and Roddick (1994) have observed that Pb is preferentially lost from metamict zircon during incremental heating. Metamictization is the result of U-decay which generates enough α-particles and fission products (Woodhead et al. 1991), progressively to destroy the zircon lattice. This creates a 'leaky' zircon with respect to Pb and a severely metamict zircon may have a closure temperature as low as 450 °C (Cherniak et al. 1991). Thus, it has been concluded that the U-Pb system in newly formed or recrystallized zircons cannot be reset or measurably disturbed during the duration of an orogenic cycle (Mezger and Krogstad 1997) and zircon 'age' survival from source rocks during anatexis at 500–800 °C is nearly a certainty (Inger and Harris 1993; Lee et al. 1997).

Another potential problem in interpreting lower intercept discordant zircon ages is the effect of fluid circulation. In an active tectonic environment like Nanga Parbat, hot meteoric and metamorphic fluids are vigorously circulating through the crust due to the rapid uplifting rock and accompanying topographically driven hydraulic head (Craw et al. 1994). Quite distinct from diffusion, these fluids create an environment which could potentially leach Pb from zircon, dating local and recent

Table 1 Summary of U-Th-Pb isotopic data for the Jutial pluton and cross-cutting dike (*g* grain, *sp* spot, @1 refers to a subsequent analysis on an existing spot)

Age (Ma) $^{208}Pb/^{232}Th$	Age (Ma) $^{208}Pb/^{232}Th$ s.e.	$^{208}Pb^*/^{232}Th$	$^{208}Pb/^{232}Th$ s.e.	$\%^{208}Pb^*$	Th est ppm	Th/U	Grain
Jutial dike (Th-Pb monazite)							
5.14	0.12	2.54E-04	5.83E-06	85.80	1.08E + 05	17.56	J-4_gr2sp1
5.33	0.10	2.64E-04	4.99E-06	88.69	1.00E + 05	22.75	J-4_gr4sp1
5.14	0.10	2.54E-04	5.06E-06	85.44	1.28E + 05	19.47	J-4_gr5sp1
5.47	0.14	2.71E-04	7.16E-06	83.42	9.25E + 04	13.07	J-4_gr6sp1
5.70	0.12	2.82E-04	5.88E-06	89.67	5.59E + 05	10.39	J-4_gr6sp1@1
5.23	0.12	2.59E-04	5.71E-06	86.55	4.68E + 04	13.97	J-4_gr10sp1
5.46	0.11	2.70E-04	5.52E-06	87.66	8.14E + 04	12.61	J-4_gr10sp2
5.14	0.13	2.54E-04	6.33E-06	84.24	7.71E + 04	15.77	J-4_gr8sp1
7.06	0.09	3.49E-04	4.21E-06	91.49	1.08E + 05	16.19	J-4_gr1sp1
5.04	0.14	2.49E-04	6.75E-06	83.12	7.23E + 04	13.56	J-4_gr7sp2
5.27 ± 0.07 = weighted average monazite age (N = 9)							
Jutial pluton (Th-Pb monazite)							
9.20	0.15	4.55E-04	7.61E-06	93.02	1.43E + 05	23.15	J-2_gr5sp2
9.31	0.19	4.61E-04	9.55E-06	94.17	1.89E + 05	12.26	J-2_gr4sp1
9.59	0.14	4.75E-04	7.12E-06	94.68	1.37E + 05	23.13	J-2_gr2sp1
9.73	0.13	4.81E-04	6.64E-06	93.89	1.64E + 05	15.23	J-2_gr6sp1
9.79	0.15	4.85E-04	7.45E-06	93.37	1.62E + 05	13.93	J-2_gr6sp2
11.55	0.18	5.72E-04	8.79E-06	93.65	1.26E + 05	15.92	J-2_gr7sp1
9.90 ± 0.15 = weighted average monazite age (N = 6)							
9.51 ± 0.12 = weighted average monazite age (N = 5)							

Age (Ma) $^{206}Pb/^{238}U$	Age (Ma) $^{206}Pb/^{238}U$ s.e.	Age (Ma) $^{207}Pb/^{235}U$	Age (Ma) $^{207}Pb/^{235}U$ s.e.	Age (Ma) $^{207}Pb/^{206}Pb$	Age (Ma) $^{207}Pb/^{206}Pb$ s.e.	$^{206}Pb^*/^{238}U$	$^{206}Pb^*/^{238}U$ s.e.
Jutial pluton (U-Pb zircon)							
7.24	0.75	2.83	4.18	Nan	0.03	1.12E-03	1.16E-04
7.85	0.64	8.00	1.70	54.39	456.00	1.22E-03	9.98E-05
8.51	1.12	7.52	1.55	NaN	0.01	1.32E-03	1.74E-04
8.78	0.81	10.03	5.63	322.90	1200.00	1.36E-03	1.26E-04
9.11	0.67	15.08	6.44	1114.00	787.00	1.42E-03	1.04E-04
9.35	2.09	−1.11	16.60	NaN	0.08	1.45E-03	3.24E-04
9.49	0.64	10.65	4.93	282.70	998.00	1.47E-03	9.97E-05
9.52	0.58	11.28	2.75	405.40	506.00	1.48E-03	8.98E-05
9.91	0.85	11.38	8.22	333.60	1570.00	1.54E-03	1.31E-04
11.10	0.28	8.28	2.98	NaN	0.01	1.72E-03	4.31E-05
11.21	0.28	13.33	1.06	413.30	181.00	1.74E-03	4.33E-05
11.80	1.81	11.45	1.77	NaN	0.00	1.83E-03	2.81E-04
15.15	2.63	15.44	2.68	60.84	47.80	2.35E-03	4.09E-04
15.40	2.43	15.67	2.47	57.66	43.40	2.39E-03	3.78E-04
14.95	1.66	12.58	6.14	NaN	0.02	2.32E-03	2.58E-04
14.44	1.87	14.27	3.17	NaN	0.01	2.24E-03	2.91E-04
9.28	0.52	10.54	2.96	306.70	601.00	1.44E-03	8.05E-05
9.88	0.55	10.32	1.75	114.20	367.00	1.53E-03	8.56E-05

$^{207}Pb^*/^{235}U$	$^{207}Pb^*/^{235}U$ s.e.	$^{207}Pb^*/^{206}Pb^*$	$^{207}Pb^*/^{206}Pb^*$ s.e.	$\%^{206}Pb^*$	$\%^{207}Pb^*$	U est ppm	Grain
2.80E-03	4.13E-03	1.80E-02	2.62E-02	87.45	12.39	4269	J-2_gr5sp2
7.91E-03	1.68E-03	4.71E-02	8.99E-03	97.46	67.82	2700	J-2_gr1sp1@1
7.43E-03	1.54E-03	4.08E-02	6.42E-03	97.27	63.80	5492	J-2_gr3sp1
9.93E-03	5.60E-03	5.29E-02	2.80E-02	90.65	36.61	2525	J-2_gr1sp1
1.50E-02	6.43E-03	7.67E-02	3.02E-02	92.29	49.55	5472	J-2_gr7sp1
1.10E-02	1.63E-02	5.47E-02	8.19E-03	75.19	12.06	419	J-2_gr4sp2
1.06E-02	4.90E-03	5.19E-02	2.27E-02	95.14	54.45	844	J-2_gr4sp2@1
1.12E-02	2.74E-03	5.48E-02	1.24E-02	95.26	55.77	6363	J-2_gr2sp2
1.13E-02	8.19E-03	5.31E-02	3.68E-02	87.73	28.49	3357	J-2_gr5sp3
8.19E-03	2.96E-03	3.44E-02	1.20E-02	95.06	43.46	3443	J-2_gr2sp3
1.32E-02	1.06E-03	5.50E-02	4.46E-03	99.65	94.78	3384	J-2_gr2sp3@1
1.13E-02	1.76E-03	4.49E-02	1.63E-03	99.41	89.80	6134	J-2_gr3sp1@1
1.53E-02	2.67E-03	4.72E-02	9.48E-04	99.94	98.90	1449	J-2_gr3sp2
1.56E-02	2.47E-03	4.72E-02	8.59E-04	99.95	99.05	6293	J-2_gr3sp1@2

Table 1 (Contd.)

$^{207}Pb^*/^{235}U$	$^{207}Pb^*/^{235}U$ s.e.	$^{207}Pb^*/^{206}Pb^*$	$^{207}Pb^*/^{206}Pb^*$ s.e.	$\%^{206}Pb^*$	$\%^{207}Pb^*$	U est ppm	Grain
1.25E-02	6.12E-03	3.90E-02	1.82E-02	91.61	77.23	2755	J-1_gr1sp2
1.42E-02	3.16E-03	4.58E-02	8.39E-03	96.28	68.12	5415	J-1_gr4sp1
1.04E-02	2.94E-03	5.25E-02	1.38E-02	94.52	51.18	2999	J-1_gr7sp3
1.02E-02	1.74E-03	4.83E-02	7.51E-03	98.19	75.25	3083	J-1_gr7sp3@1
9.54 ± 0.37 = weighted average $^{206}Pb/^{238}U$ zircon age (N = 14)							
9.39 ± 0.13 = weighted average $^{206}Pb/^{238}U$ zircon age (N = 8)							

Table 2 Summary U-Th-Pb isotopic data for the Mazeno Pass pluton (*g* grain, *sp* spot, @1 refers to a subsequent analysis on an existing spot)

Age (Ma) $^{208}Pb/^{232}Th$	Age (Ma) $^{208}Pb/^{232}Th$ s.e.	$^{208}Pb^*/^{232}Th$	$^{208}Pb^*/^{232}Th$ s.e.	$\%^{208}Pb^*$	Th est ppm	Th/U	Grain
Mazeno Pass pluton (Th-Pb monazite)							
1.21	0.11	5.97E-05	5.40E-06	52.02	9.09E + 04	18.79	MAZ_gr4sp1
1.53	0.08	7.59E-05	4.12E-06	65.58	1.61E + 05	16.34	MAZ_gr3sp1
1.59	0.07	7.88E-05	3.65E-06	67.48	1.89E + 05	14.86	MAZ_gr2sp1
1.45	0.07	7.19E-05	3.63E-06	63.68	1.99E + 05	15.61	MAZ_gr3sp2
1.64	0.07	8.12E-05	3.61E-06	69.77	1.54E + 05	16.32	MAZ_gr4sp2
1.36	0.08	6.72E-05	4.06E-06	65.01	1.35E + 05	17.35	MAZ_gr2sp2
3.31	0.09	1.64E-04	4.55E-06	82.78	2.04E + 05	22.83	MAZ_gr1sp1
3.33	0.08	1.65E-04	3.97E-06	83.23	1.73E + 05	22.33	MAZ_gr1sp2
1.44 ± 0.06 = weighted average monazite age (N = 6)							

Age (Ma) $^{206}Pb/^{238}U$	Age (Ma) $^{206}Pb/^{238}U$ s.e.	Age (Ma) $^{207}Pb/^{235}U$	Age (Ma) $^{207}Pb/^{235}U$ s.e.	Age (Ma) $^{207}Pb/^{206}Pb$	Age (Ma) $^{207}Pb/^{206}Pb$ s.e.	$^{206}Pb^*/^{238}U$	$^{206}Pb^*/^{238}U$ s.e.
Mazeno Pass pluton (U-Pb zircon)							
1.22	0.08	0.73	0.69	NaN	0.03	1.90E-04	1.24E-05
1.30	0.08	0.63	0.97	NaN	0.03	2.02E-04	1.24E-05
1.36	0.11	2.35	1.36	1193.00	1060.00	2.10E-04	1.74E-05
1.43	0.15	1.59	2.67	252.90	3710.00	2.22E-04	2.39E-05
251.20	7.20	462.00	56.90	1717.00	252.00	3.97E-02	1.16E-03
413.90	14.70	695.70	51.40	1759.00	162.00	6.63E-02	2.43E-03
858.90	75.50	1181.00	70.10	1830.00	68.70	1.43E-01	1.34E-02
891.00	94.90	1201.00	84.00	1812.00	45.50	1.48E-01	1.69E-02
1210.00	29.70	1485.00	37.30	1903.00	63.50	2.07E-01	5.56E-03
1362.00	60.40	1519.00	62.30	1745.00	97.10	2.35E-01	1.16E-02
1399.00	51.30	1599.00	33.00	1874.00	34.90	2.42E-01	9.88E-03
1760.00	39.00	1800.00	26.50	1850.00	38.90	3.13E-01	1.23E-02
1816.00	94.00	1860.00	84.50	1910.00	112.00	3.25E-01	1.93E-02

$^{207}Pb^*/^{235}U$	$^{207}Pb^*/^{235}U$ s.e.	$^{207}Pb^*/^{206}Pb^*$	$^{207}Pb^*/^{206}Pb^*$ s.e.	$\%^{206}Pb^*$	$\%^{207}Pb^*$	U est ppm	Grain
7.21E-04	6.83E-04	2.76E-02	2.54E-02	91.49	25.89	9409	MAZ_gr7sp2@1
6.20E-04	9.56E-04	2.23E-02	3.35E-02	90.58	20.10	6267	MAZ_gr7sp1@1
2.32E-03	1.34E-03	7.98E-02	4.27E-02	84.80	33.24	8982	MAZ_gr7sp2
1.57E-03	2.63E-03	5.13E-02	8.28E-02	72.75	12.75	5930	MAZ_gr7sp1
5.76E-01	8.84E-02	1.05E-01	1.44E-02	94.00	65.47	566	MAZ_gr4sp3
9.84E-01	1.00E-01	1.08E-01	9.56E-03	96.54	77.58	468	MAZ_gr9sp1
2.20E + 00	2.21E-01	1.12E-01	4.24E-03	98.02	86.50	296	MAZ_gr5sp1
2.26E + 00	2.70E-01	1.11E-01	2.77E-03	99.67	97.50	307	MAZ_gr5sp1@1
3.32E + 00	1.58E-01	1.17E-01	4.12E-03	98.28	88.53	211	MAZ_gr6sp1
3.46E + 00	2.74E-01	1.07E-01	5.66E-03	97.46	82.55	214	MAZ_gr4sp1
3.83E + 00	1.57E-01	1.15E-01	2.22E-03	99.27	94.74	228	MAZ_gr4sp1@1
4.89E + 00	3.87E-01	1.13E-01	4.23E-03	98.30	93.57	250	MAZ_gr8sp1
5.25E + 00	5.20E-01	1.17E-01	7.32E-03	97.78	85.55	116	MAZ_gr4sp2
1.35 ± 0.05 = weighted average $^{206}Pb/^{238}U$ zircon age (N = 4)							

fluid flow. In many geochronologic studies, other accessory minerals such as monazite are used to constrain the lower intercept defined by the zircon discordia more precisely (e.g. Machado et al. 1990; Schärer et al. 1994). Similar to our analyses of the Jutial pluton, we analyzed monazites as well as zircons from sample E610-A using

the ion microprobe at UCLA (Table 2). Monazite from the Mazeno Pass pluton yielded a weighted mean $^{208}Pb/^{232}Th$ age of 1.44 ± 0.06 Ma. One monazite grain yielded slightly older ages (~3 Ma) and is interpreted as representing an inherited component of an unidentified source; protracted, petrologically variable melts at Mazeno Pass are evident by the pegmatites and cordierite-bearing bodies in the area. Accordingly, we take 1.40 ± 0.05 Ma as the intrusion age of the Mazeno Pass pluton and interpret the discordant zircon data as representing a two-component system consisting of Quaternary magmatic overgrowths on older inherited or xenocrystic Proterozoic zircon cores. This is consistent with images obtained through BSE/SEM of our analyzed zircons and what is now a multitude of ion microprobe studies of zircon U-Pb systematics (e.g. Miller et al. 1998).

Discussion

Our geochronologic results indicate a disparity in pluton ages across the massif: in the north, the Jutial pluton gives a crystallization age of 9.5 Ma, with no detected inherited Proterozoic component, and to the south, both the Tato (Zeitler et al. 1993) and Mazeno plutons give 1–1.5 Ma crystallization ages with pronounced Proterozoic inheritance. The younger leucogranite ages to the south, together with younger basement cooling ages and deeper metamorphic assemblages in the south (Winslow et al. 1995, 1996), indicate either (1) an abrupt, ~10 million year southward younging of massif events or (2) a deeper exposed part of the massif centered over the summit region. We favor the latter which is consistent with the first order structural observation that the massif is a north-plunging fold (Treloar et al. 1991; Winslow et al. 1995; Edwards et al. 1996) associated with a crustal-scale pop-up structure (Edwards 1998; Schneider et al. in press), whereby the deepest and youngest exposures are in the south. Leucogranite generation most likely began when Proterozoic migmatites and gneisses underwent partial melting through fluid-absent muscovite breakdown at temperatures of ~700 °C (Butler et al. 1997). Further, according to Butler and coworkers, the source would have been at pressures around 7 kbar for melting to occur on the fluid absent solidus. Fluid absent conditions allowed the melt to ascend through the crust before crystallization (Butler et al. 1997).

The arrest of melt ascent may not be so easily explained. Emplacement has frequently been explained as the consequence of a density equilibration between rising magma and the surrounding rock where magma is emplaced at a level of neutral buoyancy. In spite of the common belief that overall density controls magma entrapment, it is difficult to fathom such a mechanism for the granites at Nanga Parbat. Amphibolite-grade lithologies within the NPHM are locally migmatitic and include both orthogneisses and paragneisses. These rocks are predominantly low-Al gneisses, but also contain minor interbedded amphibolite and calc-silicate granulite. The composition of the granites is largely the same as the orthogneiss from which they originated and which they intrude. Also there are no apparent differences within the country rock that would suggest a density contrast. We therefore look to a more complex structural setting to explain the mechanical control of pluton emplacement. Throughout the massif, there are numerous local shear zones mapped (Madin et al. 1989; Treloar et al. 1991; Winslow et al. 1996; Edwards et al. 1996, 1997; Edwards 1998), which would allow the rise and entrapment of the plutons and are considered in the next sections.

Plutonism and shear zone association

The role of shear zones in focusing and volumetrically accommodating magma displacement and emplacement has been reported by numerous workers (e.g. Brown 1994) and the inherent relationship between faulting and crustal-scale strength heterogeneities (e.g. England and Houseman 1985) are both well established. Hanmer (1997) proposed that initial shear zone development guides the emplacement of hot melts into the surrounding crust where the resulting thermal anomaly leads to extensive melting and further production of granitoids. Conversely, the influence of magma entrapment on structures developed during tectonism has also been the focus of many studies (e.g. Hollister and Crawford 1986; Lister and Baldwin 1993), where it is suggested that deformation is localized adjacent to, and along the walls of, the pluton as a result of thermal weakening of the country rock creating a high strain domain. Thus as it nears the point of crystallization, the subsolidus pluton represents a focused zone of thermally softened material, capable of deforming readily. Hollister and Crawford (1986) suggested that plutonism facilitated deformation in ductile shear zones in a contractional setting whereby melt intrusions reduce the shear stress of the planes of failure and enabling the shear zone to propagate. Positive feedback allows continuation of this process leading to large-scale crustal displacement.

Our field mapping show the young plutonism at NPHM is spatially associated with the major shear zones of the massif, consistent with recent preliminary work (Butler et al. 1997). The Mazeno Pass pluton, one of the larger bodies, intruded the northwest margin of a major NPHM shear zone (the Rupal shear zone) that was responsible for accommodating much of the uplift of Nanga Parbat in the south (Edwards et al. 1996; Edwards 1998). The segregation and migration of the source melt for the Mazeno Pass pluton may have been due to the Rupal shear zone. Although the pluton is undeformed, it is small and intrudes young (Schneider unpub data) and recently deformed orthogneiss. The Jutial pluton is similarly recognized as one of several deformed to undeformed granite bodies intruded along the western margin of the massif (Butler et al. 1992; George et al. 1993). The pluton is an undeformed granite which is discordant to

local foliation as well as the adjacent trace of the Main Mantle Thrust. Local mapping and satellite image interpretation (A. Pêcher personal communication) indicate that it is located in the tip of an older splay of the Raikot fault. Due to the onset of rapid uplift coeval with the emplacement of the Jutial pluton (ca. 10 Ma), higher strain rates are likely to have operated and thus facilitated melt supply, segregation, migration, and emplacement into shallower portions of the crust by exploitation of fractures associated with the fault system. For both the Mazeno Pass and Jutial pluton, we propose predominantly shear zone guided intrusion as the mechanism for entrapment and we further suggest this may have operated for all the larger leucogranites at Nanga Parbat. Synchronism of granite emplacement, deformation and metamorphism, as seen within the massif, suggests that granite injection is associated with localized deformation (Schneider et al. 1998). It is remarkable, however, that the majority of each of the plutons remained undeformed by the pervasive ductile deformation. Hollister and Crawford (1986) have shown that undeformed plutons can represent syn-deformational melt localized and later crystallized along zones of major crustal displacement. We suggest that the Mazeno Pass and Jutial plutons represents part of the overall snapshot of deformation at Nanga Parbat where local granites are generated and emplaced within the broad shear zones where the shear zones create space for migrating magma.

Depth of emplacement and exhumation implications

In addition to granitic intrusion and entrapment along larger shear zones, we also suggest that the granites were influenced by rheologic stratification in the crust. Typically, the maximum crustal strength occurs at or near the ductile-brittle transition. Along with the thermal structure of the crust, the ductile-brittle transition is also elevated by rapid uplift and may occur at depths as shallow as 6–7 km, as shown in the Southern Alps of New Zealand (Koons 1987; Holm et al. 1989). An elevated ductile-brittle transition is also indicated within NPHM by fluid inclusion studies (Craw et al. 1994) and petrologic and geochemical observations (Butler et al. 1997) that together indicate that the ductile-brittle transition lies about 7 ± 1 km below the (notably non-horizontal) surface. Seismological results also reveal a present-day seismic cutoff zone at the near surface (~7 km) with a lack of shallow seismic events below this depth within Nanga Parbat (Meltzer et al. 1998). Although large spatial and temporal fluctuations in the depth of the brittle-ductile transition are likely in dynamically evolving areas like Nanga Parbat (due e.g. to large fluid pressure changes, seismic unloading, etc.), we take 6–7 km as the general depth estimate for the recent depth of the ductile-brittle transition at NPHM.

Two lines of evidence exist for the emplacement of the Mazeno Pass pluton at ~7 km: (1) accepting the 1.4 Ma crystallization age for the Mazeno Pass pluton and back-calculating assuming an average exhumation rate of 4.5–5 km per million years (Zeitler 1985; Zeitler et al. 1993; Winslow et al. 1994; Whittington 1996) places the pluton at a depth of 6–7 km at ~1.5 Ma, similar to our estimated depth of the ductile-brittle transition, and (2) biotite $^{40}Ar/^{39}Ar$ cooling ages are 2–4 Ma from Mazeno Pass and Upper Rupal (Schneider et al. 1997; Schneider unpublished data); the closure temperature for these micas is probably ~400 °C since closure temperatures for argon diffusion at extremely fast cooling rates (here, due to rapid denudation) are typically elevated (Baldwin et al. 1993). Since the crystallization age of the pluton is surprisingly younger than the basement mica cooling ages, the Mazeno pluton was intruded into relatively cool (< 400 °C) basement rocks. In addition, Craw et al. (1994) and Winslow et al. (1994) illustrated that the rapid denudation of Nanga Parbat resulted in the advection of isotherms to shallow crustal levels causing an elevated geotherm of 60–70 °C/km in upper crustal levels. If correct, this also indicates the pluton crystallized at 6–7 km and we conclude that this is the minimum depth of emplacement. A similar environment exists in Tato valley where the crystallization of the Tato pluton is slightly younger then local basement cooling (Zeitler et al. 1993; Winslow et al. 1996).

The presence of granites in and around 6–7 km probably impeded the deep penetration of meteoric fluids circulating within the massif as suggested by stable isotope data (Chamberlain et al. 1995). Local fluid infiltration, particularly within shear zones, into biotite-rich metapelites is suggested to have triggered melting leading to anatectic textures and the formation of cordierite seams (Butler et al. 1997). In a recent study, Whittington et al. (1999) observe that the 1–2 Ma larger leucogranite bodies (e.g. Tato, Mazeno) and thin sheets (dikes in Tato, Rupal) are cross-cut by metasomatic or restitic cordierite seams. Thermobarometry on these seams indicate that they formed at 3.0 ± 0.4 kbar (300 ± 40 MPa) and 630° ± 50 °C (Whittington et al. 1999). If this is the case, the 1–2 Ma leucogranites are required to have crystallized at 10 km depth for the cordierite seams to form and cross-cut the leucogranites. This requires exhumation rates as high as 10 km per million years. Our proposed depth for the emplacement of the granites is slightly shallower then that inferred by Whittington et al. (1999) and is more consistent with reported exhumation rates (i.e. 4–5 km per million years; Zeitler 1985; Zeitler et al. 1993; Winslow et al. 1994; Whittington 1996).

Conclusions

The Mazeno Pass pluton yielded concordant U-Pb zircon rim ages of 1.35 ± 0.05 Ma and Th-Pb monazite ages of 1.44 ± 0.06 Ma. The Jutial pluton yielded concordant U-Pb zircon and Th-Pb monazite ages of 9.39 ± 0.13 Ma and 9.51 ± 0.12, respectively. Based on consistency in each case between the isotopic tech-

niques, we interpret these ages as recording the respective crystallization ages of each pluton. The Jutial pluton was subsequently intruded by smaller leucogranites at 5.3 Ma. All these ages are young for typical High Himalayan leucogranites. With these new geochronologic results and field observations, we suggest a dynamic association between Nanga Parbat's major shear zones and plutonism, with an appropriate limiter for ascending partial melt (e.g. the ductile-brittle transition) further influencing pluton entrapment. Coeval plutonism, metamorphism and deformation appear to be linked spatially as well as temporally suggesting a feedback relationship between anatexis and deformation. At Nanga Parbat, these processes couple together producing rapid uplift, that probably initiated in the Late Miocene. Our new geochronology indicates a fundamental link between plutonism, metamorphism and deformation.

Acknowledgements This work was supported by the Continental Dynamics division of the National Science Foundation (EAR 9418849 to PKZ). We thank Arnaud Pêcher, Mark Harrison, Bill Kidd and Patrick Le Fort for their insightful discussions both in the field and the lab. This paper benefitted greatly from reviews by Ian Williams and Alan Whittington. Alicia Stanfill, Mitch Wemple, and Anton Seimon provided essential field assistance. Kathy Repa (Material Sciences, Lehigh) helped with the SEM.

References

Amato JM, Wright JE, Gans PB, Miller EL (1994) Magmatically induced metamorphism and deformation in the Kigluaik gneiss dome, Seward Peninsula, Alaska. Tectonics 13: 515–527

Baldwin S, Lister G, Hill EJ, Foster D, McDougall I (1993) Thermochronologic constraints on the tectonic evolution of active metamorphic core complexes, D'Entrecasteax Island, Papua New Guinea. Tectonics 12: 611–628

Barth S, Oberli F, Martin M (1989) U-Th-Pb systematics of morphologically characterized zircon and allanite: a high resolution isotopic study of the Alpine Resen pluton (northern Italy). Earth Planet Sci Lett 95: 235–254

Brown M (1994) The generation, segregation, ascent and emplacement of granite magma: the migmatite-to-crustally-derived granite connection in thickened orogens. Earth-Sci Rev 36: 83–130

Butler R, Prior D (1988) Anatomy of a continental subduction zone: the Main Mantle Thrust in northern Pakistan. Geol Rundsch 77: 235–255

Butler R, Prior D, Knipe R (1989) Neotectonics of the Nanga Parbat syntaxis, Pakistan, and crustal stacking in the northwest Himalaya. Earth Planet Sci Lett 94: 329–343

Butler R, George M, Harris N, Jones C, Prior D, Treloar P, Wheeler J (1992) Geology of the northern part of the Nanga Parbat massif, northern Pakistan, and its implications for Himalyan tectonics. J Geol Soc London 149: 557–567

Butler R, Harris N, Whittington A (1997) Interactions between deformation, magmatism and hydrothermal activity during active crustal thickening: a field example from Nanga Parbat, Pakistan. Mineral Mag 61: 37–51

Chapman H, Roddick J (1994) Kinetics of Pb release during zircon evaporation technique. Earth Planet Sci Lett 121: 601–611

Chamberlain CP, Zeitler PK, Barnett D, Winslow D, Poulson S, Leahy T, Hammer J (1995) Active hydrothermal systems during the recent uplift of Nanga Parbat. J Geophys Res 100: 439–453

Cherniak D, Lanford W, Ryerson F (1991) Lead diffusion in apatite and zircon using ion implantation and Rutherford backscattering techniques. Geochim Cosmoschim Acta 55: 1663–1673

Claoue-Long JC, Sobolev NN, Shatsky VS, Sobolev AV (1991) Zircon response to diamond-pressure metamorphism in the Kokchetav Massif, USSR. Geology 19: 710–713

Coward MP, Jan MQ, Rex D, Tarney J, Thirwall M, Windely BF (1982) The tectonic history of Kohistan and its implications for Himalayan structure. J Geol Soc London 139: 299–308

Craw D, Koons PO, Winslow D, Chamberlain CP, Zeitler PK (1994) Boiling fluids in a region of rapid uplift, NPHM, Pakistan. Earth Planet Sci Lett 128: 169–182

Debon F, Zimmermann J, Liu GH, Jin CW, Xu RH (1985) Time relationship between magmatism, tectonics and metamorphism in southern Tibet: new K-Ar data. Geol Rundch 74: 229–236

Deer W, Howie R, Zussman J (1966) An introduction to the rock forming minerals. Longman, London

Edwards MA (1998) Examples of tectonic mechanisms for local contraction and exhumation of the leading edge of India, southern Tibet and Nanga Parbat, Pakistan. PhD dissertation, State University of New York at Albany

Edwards MA, Harrison TM (1997) When did the roof collapse? Late Miocene north-south extension in the high Himalaya revealed by Th-Pb monazite dating of the Khula Kangri granite. Geology 25: 543–546

Edwards MA, Kidd W, Seeber L, Pêcher A, Le Fort L, Riaz M, Khan MA (1996) An upwardly mobile indentor? The Nanga Parbat-Haramosh Massif viewed as a crustal-scale pop-up structure. EOS Trans Am Geophys Union 236: F692

Edwards MA, Kidd W, Khan MA, Schneider D, Zeitler PK (1997) Structural geology of the southwestern margin of Nanga Parbat. EOS Trans Am Geophys Union 237: F651

England P, Houseman G (1985) Role of lithospheric strength heterogeneities in the tectonics of Tibet and neighbouring regions. Nature 315: 297–301

Fielding E (1996) Tibet uplift and erosion. Tectonophysics 260: 55–84

George M, Harris N, Butler R (1993) The tectonic implications of contrasting granite magmatism between the Kohistan island arc and the NPHM, Pakistan Himalaya. In: Treloar P, Searle M (eds) Himalaya tectonics. Geol Soc London Spec Pub 74: 173–191

George M, Reddy R, Harris N (1995) Isotopic constraints on the cooling history of the NPHM and Kohistan arc, western Himalaya. Tectonics 14: 237–252

Hanmer S (1997) Shear zone reactivation at granulite facies: the importance of plutons in the localization of viscous flow. J Geol Soc London 154: 111–116

Harris N, Massey J (1994) Decompression and anatexis of Himalayan metapelites. Tectonics 13: 1537–1546

Harrison TM, Watson EB (1983) Kinetics of zircon dissolution and zirconium diffusion in granitic melts of variable water content. Contrib Mineral Petrol 84: 66–72

Harrison TM, McKeegan K, LeFort P (1995) Detection of inherited monazite in the Manaslu leucogranite by $^{208}Pb/^{232}Th$ ion microprobe dating: crystallization age and tectonic implications. Earth Planet Sci Lett 133: 271–282

Harrison TM, Grove M, Lovera O, Catlos E (1998) A model for the origin of Himalayan anatexis and inverted metamorphism. J Geophys Res 103: 27017–27032

Herren E (1987) The Zanskar shear zone: northeast-southwest extension within the Higher Himalayas (Ladakh, India). Geology 15: 409–413

Hill EJ, Baldwin S, Lister G (1992), Unroofing of active metamorphic core complexes in the D'Entrecasteaux Islands, Papua New Guinea. Geology 11: 261–277

Hollister L, Crawford M (1986) Melt-enhanced deformation: a major tectonic process. Geology 14: 558–561

Holm D, Norris RJ, Craw C (1989) Brittle and ductile deformation in a zone of rapid uplift: Central Southern Alps, New Zealand. Tectonics 8: 153–168

Inger S, Harris N (1993) Geochemical constraints on leucogranite magmatism in the Langtang Valley, Nepal Himalaya. J Petrol 23: 234–247

Jaupart C, Provost A (1985) Heat focussing, granite genesis and inverted metamorphic gradients in continental collision zones. Earth Planet Sci Lett 73: 385–397

Koons PO (1987) Some thermal and mechanical consequences of rapid uplift; an example from the Southern Alps, New Zealand. Earth Planet Sci Lett 86: 307–319

Lee J, Williams IS, Ellis D (1997) Pb, U, Th diffusion in natural zircon. Nature 390: 159–161

Le Fort P (1975) Himalaya: the collided range. Present knowledge of the continental arc. Am J Sci 275: 1–44

Le Fort P (1981) Manaslu leucogranite: a collision signature of the Himalaya. A model for its genesis and emplacement. J Geophys Res 86: 10545–10568

Le Fort P, Cuney M, Deniel C, France-Lanord C, Sheppard S, Upreti BN, Vidal P (1987) Crustal generation of Himalayan leucogranite. Tectonophysics 134: 39–57

Lister J, Baldwin S (1993) Plutonism and the origin of metamorphic core complexes. Geology 21: 607–610

Machado N, Krogh T, Weber W (1990) U-Pb geochronology of basement gneisses in the Thompson Belt (Manitoba); evidence for pre-Kenoran and Pikwitonei-type crust and early Proterozoic basement reactivation in the western margin of the Archean Superior Province. Can J Earth Sci 27: 794–802

Madin IP (1986) Structure and neotectonics of the northwestern NPHM. MSc thesis, Oregon State University

Madin IP, Lawrence R, Ur-Rehman S (1989) The northwestern Nanga Parbat massif: evidence for crustal uplift at the northwestern corner of the Indian craton. Geol Soc Am Spec Pap 232: 169–182

Meltzer A, Sarker G, Seeber L, Armbruster J (1998) Snap, Crackle, Pop! Seismicity and crustal structure at Nanga Parbat, Pakistan Himalaya. EOS Trans Am Geophys Union 79: F909

Mezger K, Krogstad E (1997) Interpretation of discordant U-Pb zircon ages: An evaluation. J Metamorphic Geol 15: 127–140

Miller C, Hatcher R, Harrison TM, Coath C, Gorisch E (1998) Cryptic crustal events elucidated through zone imaging and ion microprobe studies of zircon, southern Appalachian Blue Ridge, North Carolina-Georgia. Geology 26: 419–422

Misch P (1949) Metasomatic granitization of batholithic dimensions. Am J Sci 247: 209–249

Molnar P, England P, Martinod J (1993) Mantle dynamics, the uplift of the Tibetan plateau, and the Indian monsoon. Review Geophys 31: 357–396

Murphy M, Harrison TM (1998) The relationship between leucogranites and the STDS in the Rongbuk Valley, southern Tibet. EOS Trans Am Geophys Union 79: F815

Scaillet B, Pichavant M, Roux J (1991) Tourmaline, biotite and muscovite stability in felsic peraluminous liquids. EOS Trans Am Geophys Union 72: 311

Scaillet B, Pêcher A, Rochette P, Champenois M (1995) The Gangotri granite (Garhwal Himalaya): laccolithic emplacement in an extending collisional belt. J Geophys Res 100: 585–607

Schärer U, Zang LS, Tapponier P (1994) Duration of strike-slip movement in large shear zones: the Red River belt, China. Earth Planet Sci Lett 126: 438–451

Schneider D, Zeitler P, Edwards M, Kidd W (1997) Geochronological constraints on the geometry and timing of anatexis and exhumation at Nanga Parbat: a progress report. EOS Trans Am Geophys Union 237: S312

Schneider D, Edwards M, Kidd W, Zeitler P, Coath C (1998) Synkinematic magmatism within SW Nanga Parbat, Pakistan Himalaya. Geol Soc Am Abstr 30: A357

Schneider D, Edwards M, Kidd W, Zeitler P, Coath C (1999) Early Miocene anatexis identified in the western syntaxis, Pakistan Himalaya. Earth Planet Sci Lett 167: 121–129

Schneider D, Edwards M, Kidd W, Khan MA, Seeber L, Zeitler P (1999) Active tectonics of Nanga Parbat, western Himalaya: synkinematic plutonism within the doubly-vergent shear zones of a crustal-scale pop-up structure. Geology (in press)

Smith H, Chamberlain CP, Zeitler PK (1992) Documentaion of Neogene regional metamorphism in the Himalayas of Pakistan using U-Pb in monazite. Earth Planet Sci Lett 113: 93–105

Smith H, Giletti B (1997) Lead diffusion in monazite. Geochim Cosmoschim Acta 61: 1047–1055

Sobolev NN, Shatsky VS (1990) Diamond inclusions in garnets from metamorphic rocks: a new environment for diamond formation. Nature 343: 742–746

Solar G, Pressley R, Brown M, Tucker R (1998) Granite ascent in convergent orogenic belts: testing a model. Geology 26: 711–714

Tahirkheli RAK, Mattauer M, Proust F, Tapponnier P (1979) The India-Eurasia suture zone in northern Pakistan: some new data for an interpretation at plate scale. In: A. Farrah and K. DeJong (Eds) Geodynamics of Pakistan. Geol Survey Pakistan, Quetta, pp 130–135

Treloar P, Broughton RD, Williams MP, Coward MP, Windely BF (1989) Deformation, metamorphism and imbrication of the Indian plate, south of the MMT, north Pakistan. Metamorphic Geol 7: 111–125

Treloar P, Potts G, Wheeler J, Rex DC (1991) Structural evolution and asymmetric uplift of the NP syntaxis, Pakistan Himalaya. Geol Rundsch 80: 411–428

Wadia DN (1932) Notes on the geology of Nanga Parbat (Mt Diamir) and ajoining portions of Chilas, Gilgit district, Kashmir. Records Geol Surv India 66: 212–234

Watson EB, Harrison TM (1983) Zircon saturation revisited: temperature and composition effects in a variety of crustal magma types. Earth Planet Sci Lett 64: 295–304

Whittington A (1996) Exhumation overrated at Nanga Parbat. Tectonophysics 206: 215–226

Whittington A, Harris N, Butler B (1999) Contrasting anatectic styles at Nanga Parbat, northern Pakistan. Geol Soc Am Spec Pap 328: 123–145

Williams IS (1992) Some observations on the use of zircon U-Pb geochronology on the study of granitic rocks. Trans R Soc Edinburgh: Earth Sciences 83: 447–458

Winslow D, Zeitler PK, Chamberlain CP, Hollister L (1994) Direct evidence for a steep geotherm under conditions of rapid denudation, western Himalaya, Pakistan. Geology 22: 1075–1078

Winslow D, Chamberlain CP, Zeitler PK (1995) Metamorphism and melting of the lithosphere due to rapid denudation, NPHM Himalaya. J Geol 103: 395–409

Winslow D, Zeitler PK, Chamberlain CP, Williams IS (1996) Geochronologic constraints on syntaxial development in the NPHM, Pakistan. Tectonics 15: 1292–1308

Woodhead JA, Rossman GR, Silver T (1991) The metamictization of zircon: radiation dose dependent structural characteristics. Am Mineral 76: 74–82

Zeitler PK (1985) Cooling history of the NW Himalaya, Pakistan. Tectonics 4: 127–151

Zeitler PK, Chamberlain CP (1991) Petrogenetic and tectonic significance of young leucogranites from the NW Himalaya, Pakistan. Tectonics 10: 729–741

Zeitler PK, Sutter J, Williams IS, Zartman RE, Tahirkheli RAK (1989) Geochronology and temperature history of the NPHM, Pakistan. Geol Soc Am Spec Pap 232: 1–23

Zeitler PK, Chamberlain CP, Smith H (1993) Synchronous anatexis, metamorphism, and rapid denudation at Nanga Parbat, Pakistan Himalaya. Geology 21: 347–350